

Simultaneous Deep Tunneling and Classical Hopping for Hydrogen Diffusion on Metals

Wei Fang,¹ Jeremy O. Richardson,^{2,*} Ji Chen,³ Xin-Zheng Li,^{4,†} and Angelos Michaelides^{3,‡}

¹Thomas Young Centre, London Centre for Nanotechnology and Department of Chemistry, University College London, London WC1E 6BT, United Kingdom

²Laboratory of Physical Chemistry, ETH Zurich, CH-8093 Zurich, Switzerland

³Thomas Young Centre, London Centre for Nanotechnology and Department of Physics and Astronomy, University College London, London WC1E 6BT, United Kingdom

⁴School of Physics and the Collaborative Innovation Center of Quantum Matters, Peking University, Beijing 100871, People's Republic of China

(Received 9 March 2017; revised manuscript received 5 May 2017; published 19 September 2017)

Hydrogen diffusion on metals exhibits rich quantum behavior, which is not yet fully understood. Using simulations, we show that many hydrogen diffusion barriers can be categorized into those with parabolic tops and those with broad tops. With parabolic-top barriers, hydrogen diffusion evolves gradually from classical hopping, to shallow tunneling, to deep tunneling as the temperature (T) decreases, and noticeable quantum effects persist at moderate T . In contrast, with broad-top barriers quantum effects become important only at low T and the classical-to-quantum transition is sharp, at which classical hopping and deep tunneling both occur. This coexistence indicates that more than one mechanism contributes to the quantum reaction rate. The conventional definition of the classical-to-quantum crossover T is invalid for the broad tops, and we give a new definition. Extending this, we propose a model to predict the transition T for broad-top diffusion, providing a general guide for theory and experiment.

DOI: 10.1103/PhysRevLett.119.126001

Hydrogen (H) diffusion on surfaces is fundamental in disciplines such as surface science, astrophysics, and catalysis [1–9]. Because of the light mass of hydrogen, the process can exhibit significant quantum nuclear effects, such as tunneling and isotope effects. The development of surface-sensitive techniques means that it is possible to characterize these diffusion processes with high resolution, and to understand the quantum nature of hydrogen diffusion [10–13]. Various techniques have been applied, including field emission microscopy (FEM) [10], laser optical diffraction (LOD) [11], scanning tunneling microscopy (STM) [12], and helium spin echo (HeSE) [13]. Generally, such measurements have been performed on metals because these afford the opportunity of examining diffusion on ultraclean and atomically flat surfaces, which give the greatest opportunity of revealing fundamental insight of broad relevance.

Several impressive experimental studies have been performed for H and, at times, deuterium (D) on substrates such as Ni [10,11,14], Cu [12,15], Pt [16,17], and Ru [18]. Diffusion rates have been measured and, upon examining how the rates vary with temperature (T), qualitatively different behavior has been seen when moving from one substrate to another. Relatively straightforward behavior is seen on, e.g., Pt(111) where, according to HeSE measurements, the rate drops as T is lowered [17]. On Ru (0001), a gradual transition from Arrhenius behavior to a T -independent regime has been reported [18]. However, on Ni(100) [10] and Cu(100) [12], diffusion rates suddenly become T independent below a certain T , indicating a sharp

classical-to-quantum transition. Computational techniques provide complementary insight [19,20], and previous studies have helped to explain the behavior observed in specific experiments [18,21–29]. For example, the sharp transition on Ni(100) was attributed to the particular shape of the diffusion barrier [21–24]. However, previous studies have generally focused on specific surfaces, and force fields have often been used. A thorough *ab initio* comparison of hydrogen diffusion on different surfaces (including ones yet to be measured experimentally) is lacking. Moreover, a general physical understanding of surface diffusion and classical-to-quantum transitions has yet to be obtained.

In this Letter, we study hydrogen diffusion on metal surfaces with density functional theory (DFT). A key qualitative finding of this study is that many of these processes can be categorized as having barriers with conventional parabolic tops or unconventional broad tops. Of the substrates considered, parabolic-top diffusion barriers exist on Cu(111), Ni(111), and Pd(111). When T decreases, the dominant diffusion mechanism evolves gradually from classical over-the-barrier hopping, through shallow tunneling through the barrier top, to deep tunneling at the barrier bottom. Shallow tunneling enables noticeable isotope effects at moderate T (~ 200 K). Broad-top diffusion barriers exist on Ni(100), Cu(100), Ni(110), and Pd(110). For these barriers, quantum effects are important only at low T and the classical-to-quantum transition is sharp, during which classical hopping and deep tunneling coexist. In contrast to the parabolic-top barriers, a rapid onset of isotope effects is predicted for the broad-top

barriers. Theoretically, the coexistence indicates that multiple quantum transition states (TSs) can contribute to the reaction rate, providing challenges to quantum rate theories. Using the general insights obtained, we develop a simple model to predict the classical-to-quantum transition T for broad-top barriers and discuss it within the context of previous experiments and simulations.

Our DFT calculations were carried out using the VASP [30] code with the Perdew-Burke-Ernzerhof (PBE) exchange-correlation functional [31]. We use the nudged elastic band (NEB) method [32] to obtain minimum energy pathways (MEPs) for diffusion (with the substrate atoms and H free to relax in all directions). The MEPs are then used as one-dimensional (1D) potential barriers upon which the exact transmission probabilities P for incoherent tunneling are calculated by solving the Schrödinger equation [33]. There are various ways to simulate surface diffusion [19–22,28,34], e.g., assuming discrete levels [28,34]; however, for a qualitative understanding of the tunneling processes, the initial-state distribution is not crucial and depends on experimental conditions. Hence, here we use a continuous distribution for simplicity. Additionally, three Feynman path-integral (PI)-based approximate theories were tested [35], namely, ring-polymer molecular dynamics (RPMD) [36–42], thermalized microcanonical instanton (TMI) [43], and the conventional instanton method [44–48]. The 1D TMI rate is

$$k_{\text{TMI}}Z_r = \frac{1}{2\pi\hbar} \int_0^\infty e^{-W(E)/\hbar} e^{-\beta E} dE, \quad (1)$$

where $W(E) = S(\tau) - \tau E$ is the abbreviated action, S the Euclidean action of the instanton, τ its imaginary time, $E = \partial S/\partial \tau$ its energy, $\beta = 1/k_B T$, k_B the Boltzmann constant, and the scattering partition function is used for Z_r . $W(E)=0$ is used for E larger than the barrier height. The conventional instanton rate, which has been applied to gas-phase reactions [4,49–53], is the steepest-descent (SD) approximation to the integral in the TMI rate [Eq. (1)] [48]; hence, we refer to it as the SDI. In 1D, the transmission probability $e^{-W/\hbar}$ in Eq. (1) is equivalent to the WKB approximation [54]. Further details of the calculations, validation work, and tests with other functionals are provided in the Supplemental Material (SM) [55], which includes Refs. [12,16,17,23,24,32,38,43,48,54,56–64].

DFT calculations show that the diffusion barriers obtained have two different shapes [Fig. 1(a)]. Those between the threefold hollow sites on Cu(111), Ni(111), Pd(111) [Fig. 1(a)], and Ru(0001) [18] have a conventional parabolic shape near the top. Those on the (100) surface [Fig. 1(c)] of Cu and Ni, and along a path on the (110) surface [Fig. 1(b)] of Pd and Ni are, however, considerably broader. We label these barriers as parabolic top and broad top, respectively. More examples of both kinds of barriers can be found elsewhere [65]. We see that broad-top barriers

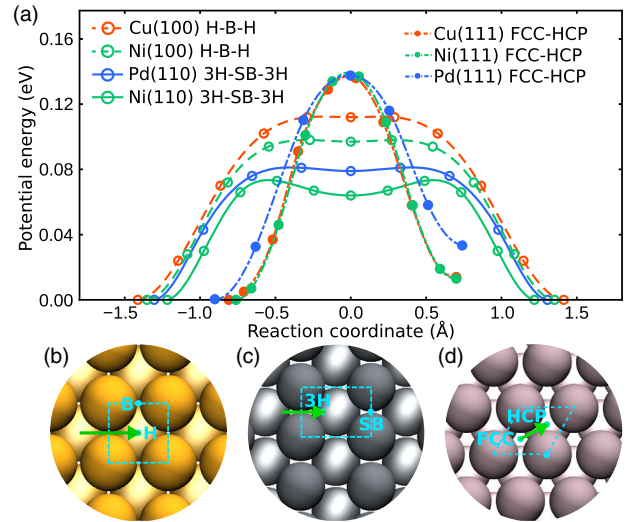


FIG. 1. (a) Energy barrier of the H diffusion paths, obtained from NEB calculations using DFT, for several transition metal surfaces. The filled symbols show data for the conventional barriers that are parabolic near the top, and the open symbols are the data points for broad-top barriers. (b) Top view of the (100) surface. (c) Top view of the (110) surface. (d) Top view of the (111) surface. Green arrows show the diffusion paths.

can occur when the adsorption sites are relatively far apart ($>2.5 \text{ \AA}$). Such barrier profiles are possible because, unlike covalent bond breaking, a strong bond between H and the continuum of metal states is maintained throughout the diffusion pathway. TSs for typical proton-transfer reaction barriers have an imaginary frequency along the reaction coordinate of circa 10^3 cm^{-1} . However, for the broad-top barriers discussed here, the TSs have almost zero imaginary frequency. In the case of Ni(110), the barrier top is even a shallow minimum.

We analyze the H diffusion mechanism across two example barriers: diffusion from a pseudothreefold hollow site over a short bridge site to another pseudothreefold hollow site (3H-SB-3H) [Fig. 1(c)] on Pd(110) is chosen as the example of a broad-top barrier. We compare it with the parabolic-top barrier found on Ni(111). The results of this analysis are shown in Figs. 2(a) and 2(d), where we plot the thermal transmission probability $P(E)e^{-\beta E}$ as a function of the incident energy E at T s above, during, and below the classical to quantum transitions. For Ni(111), the transmission mechanism changes gradually from being dominated by classical hopping, through shallow quantum tunneling, to deep quantum tunneling as T decreases [Fig. 2(a)]. At 200 K, when classical hopping is dominant, the transmission probability curve has a tail at low incident energy, meaning that shallow tunneling is also significant. For H diffusion across the 3H-SB-3H broad-top barrier on Pd(110), a different transition behavior, from classical hopping to deep tunneling, is observed. At 50 K or above, H can only classically hop over the barrier, as reflected by

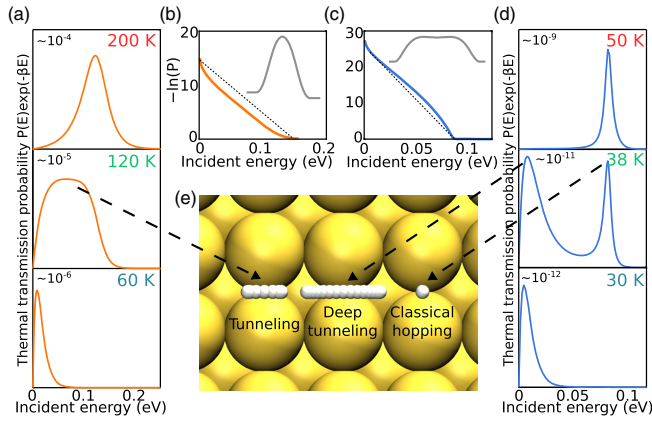


FIG. 2. Temperature dependence of H diffusion on metals for a conventional barrier that is parabolic near the top [Ni(111), left] and one that has a broad top [3H-SB-3H path Pd(110), right]. (a), (d) The exact thermal transmission probability $P(E)e^{-\beta E}$ (dimensionless) plotted against the incident energy E for the conventional barrier and the broad-top barrier, respectively. (b), (c) The transmission action (in units of \hbar) defined as $-\ln(P)$, as a function of the incident energy E for the parabolic-top barrier and the broad-top barrier. (e) Illustration of the peaks in the thermal transmission probability using tunneling paths represented by the Feynman PI.

the negligible tail of the thermal transmission probability on the low-energy side. At lower T (30 K or below), only deep quantum tunneling is allowed. However, around an intermediate transition T [38 K, middle of Fig. 2(d)] the thermal transmission probability curve has two maxima, meaning that H can deep tunnel through or classically hop over the barrier with similar probability.

To understand the origin of the anomalous tunneling, we compare the transmission action, defined as $-\hbar \ln(P)$ for the two examples. The larger the transmission action, the more difficult it is for H to tunnel through the barrier at a given incident energy. The broad-top barrier has a convex-shaped action when plotted against incident energy [Fig. 2(c)], implying that the broad barrier top hinders shallow tunneling. With a parabolic-top barrier, the action versus incident energy function is concave [Fig. 2(b)], indicating that shallow tunneling is favorable. It is the qualitatively different shapes of the transmission action curves for the two classes of barriers that leads to such different tunneling behaviors. Moreover, this distinction between the two classes of barrier enables us to define broad-top barriers precisely as those barriers for which the transmission action versus energy curve is convex. This definition is valid for all barriers considered in this study (Fig. S2 [55]), and classical hopping and deep tunneling channels coexist near the classical-to-quantum transition T when a barrier has a convex transmission action.

The coexistence of classical hopping and deep tunneling on the broad-top barrier indicates that, in contrast to the classical transition state theory picture, multiple quantum

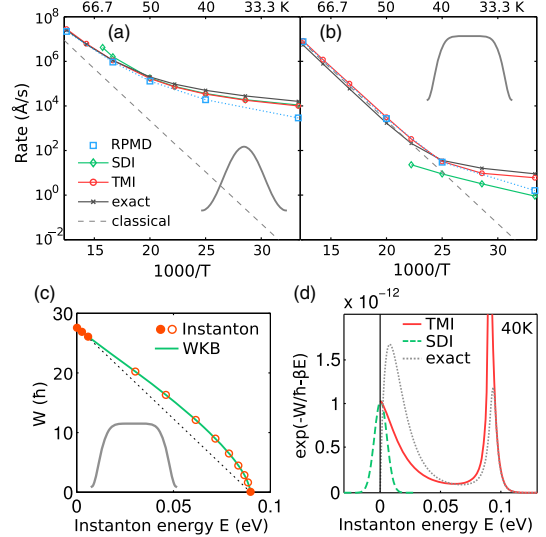


FIG. 3. Performance of different rate theories on 1D barriers (for H) with different shapes. (a) Rates on a parabolic-top barrier (inset). (b) Rates on a broad-top barrier (inset); the legend is the same as in (a). (c) The W action [Eq. (1)] plotted against energy E for the broad-top barrier in (b). The closed (open) circles show first- (second-) order saddle instantons obtained through ring-polymer instanton searches. (d) The thermal transmission probability at 40 K plotted against energy E for the barrier shown in (c) obtained using the TMI theory and using the SDI theory.

TSs can be important. To explore how well quantum rate theories describe this behavior, we analyzed a series of 1D barriers [Eq. (S3) [55]] constructed by varying the potential from a cosine (parabolic-top) shape to a broad-top one. We calculated rates using three PI-based methods [Figs. 3(a) and 3(b)], and compared them to the exact rate. On the parabolic-top barrier, all three theories perform well, agreeing with the exact rate within a factor of 3 [Fig. 3(a)]. When the barrier top is broad, TMI and RPMD rates agree with the exact rate within a factor of 2, except for the lowest T (30 K), where RPMD underestimates the rate slightly [Fig. 3(b)]. However, the SDI underestimates the rate by a factor of 3–10 in the 30–45 K range [Fig. 3(b)], and with an even wider top, the SDI underestimates the rate by 2–3 orders of magnitude. This is because the SD integral over E breaks down when the instanton is close to $E = 0$, and if multiple quantum TSs contribute. This is the case for broad-top barriers with convex W action; the instanton exists either very close to $E = 0$ or collapses at the top [Fig. 3(c)]. (Other periodic orbits do exist, but unlike normal instantons [46] these are second-order saddles of the ring-polymer potential.) Hence, the SDI does not capture the coexistence of classical hopping and deep tunneling, and fails to accurately describe the rate at low T [Fig. 3(d)]. The TMI solves these problems by avoiding the SD integral over E and instead uses several microcanonical instantons for the rate, which seems to be

a promising method for treating complex tunneling problems.

A key experimental quantity for H diffusion is the classical-to-quantum transition temperature. Its theory counterpart is the crossover T ($T_c = \hbar\omega_b/2\pi k_B$), defined using the imaginary frequency ω_b at the barrier top. However, T_c is ill defined for broad-top barriers. Here we define an alternative transition T using the W action in Eq. (1),

$$T_W = \frac{\hbar E_a}{k_B W_0}. \quad (2)$$

E_a is the classical activation energy and $W_0 = \oint \sqrt{2mV(x)}dx$, $V(x)$ is the potential. T_W is defined in this way such that $-1/k_B T_W$ is the slope of the dashed line in Fig. 3(c). This means that at T_W , the classical hopping (incident energy $E = E_a$) and deep tunneling ($E = 0^+$) have equal contributions to the diffusion rate; hence, it is the transition T to deep tunneling for broad-top barriers. For barriers with activation energy E_a and width w , Eq. (2) becomes

$$T_W = \frac{\hbar}{n_s k_B} \sqrt{\frac{E_a}{2mw^2}}, \quad 0 < n_s < 2, \quad (3)$$

where n_s is a barrier shape factor and m is the mass of hydrogen, and, on parabolic-top barriers, T_W and T_c are closely related (for derivations, see the SM [55]). For the model potentials in Eq. (S3), when the action curve becomes convex, $n_s \gtrsim 1.5$ [55]. Therefore, we used $n_s = 1.5$ and plotted Eq. (3) over a range of E_a and w [Fig. 4(a)]. This model allows one to estimate the transition T for broad-top barriers without performing rate calculations and is based only on quantities measurable in experiments, i.e., the activation energy E_a and the barrier width w .

We now use the model and insight obtained to explain and possibly predict the transition T to deep tunneling for H diffusion on several surfaces [Fig. 4(b)]. On Cu(100), STM has revealed a classical barrier for H hopping of ~ 0.2 eV and a sharp classical-to-quantum transition at 60 K [12]. Using the experimental E_a our model predicts a transition T of 56 K, in excellent agreement with experiments. Using the DFT barrier, along with the WKB approximation, the transition temperature predicted is ~ 40 K. This is still in reasonable agreement with experiments and also consistent with the simple model. On Ni(100) the experimental transition temperatures are in the 100–125 K regime [10,11]. Previous calculations using force fields have, however, led to predictions in the 40–70 K regime [21,23–26]. Both our DFT results and the model yield transition T s that are consistent with the previous simulations. Indeed, even using the experimental E_a reported (~ 0.15 eV) our model predicts a transition T of 50 K. It therefore does not seem unreasonable to suggest that an

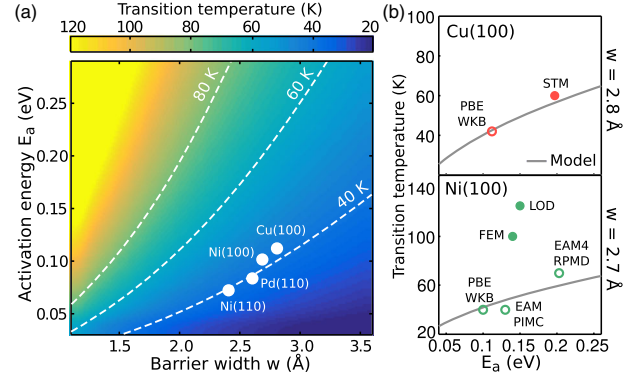


FIG. 4. (a) Transition temperature to deep tunneling [Eq. (2)] predicted by the model over a range of barrier parameters. The four broad-top barriers calculated with DFT in Fig. 1 are marked. (b) Comparison of the transition T predicted by the model with previous experiments (filled symbols) and theoretical studies (open symbols) on Cu and Ni. Previous results are taken from STM [12], FEM [10], LOD [11], PI Monte Carlo (PIMC) calculations with an embedded atom model (EAM) potential [21], and RPMD with an EAM4 potential [24]. The PBE WKB points are from this work (Fig. 1).

experimental reexamination of H diffusion on Ni(100) could be worthwhile. On Pt(111) we show in the SM that our calculations are consistent with the HeSE experiments [17,55].

Isotope effects are another important aspect of quantum diffusion and a key experimental signature of tunneling. We have examined the H-D isotope effect on a broad-top barrier and a parabolic-top barrier as a function of T . On the parabolic-top barrier, the H-D isotope effect appears at moderate T (100 K) and the rate ratio k_H/k_D increases gradually over a wide temperature range (down to 25 K). In contrast, for the broad-top barrier, no H-D isotope effect appears until T_W (~ 40 K) is reached; then, k_H/k_D increases sharply within a narrow temperature window (40–25 K). These general observations are consistent with previous studies on Ni(100) [23–25], and the qualitative difference between the two types of barriers holds for a broad range of barrier heights and widths. The sharp onset of isotope effects could, therefore, serve as an experimental signature of diffusion on a surface with broad-top barriers.

To conclude, insight into the quantum nature of hydrogen diffusion on metals has been obtained. A clear qualitative distinction between barriers with broad tops and conventional parabolic tops has been identified. For the broad-top barriers, we observed a regime at which both classical hopping and deep tunneling are favored. Despite the long history of theories for general tunneling phenomena [54,66], we are not aware of discussion of such behavior. It remains to be seen if similar behavior for hydrogen diffusion and proton transfer will be seen in other environments. Treating more complex systems will likely require a full multidimensional description of the process.

The unique behavior observed here has led to a series of general implications, including a requirement for a multi-TS theoretical treatment, a new definition of the classical to quantum transition T (T_W), and a sudden emergence of strong isotope effects around T_W .

J. C. and A. M. are supported by the European Research Council under the European Union's Seventh Framework Programme (FP/2007-2013) / ERC Grant No. 616121 (HeteroIce project). A. M. is also supported by the Royal Society through a Royal Society Wolfson Research Merit Award. X. Z. L. is supported by MOST Grant No. 2013CB934600, the National Key R&D Program under Grant No. 2016YFA0300901, and the National Science Foundation of China under Grants No. 11422431 and No. 11634001. We are grateful for computing resources provided by the London Centre for Nanotechnology, Research-Computing at University College London, and the UK's High End Computing Materials Chemistry Consortium, funded by the Engineering and Physical Sciences Research Council (Grant No. EP/L000202), for access to the ARCHER UK National Supercomputing Service.

*jeremy.richardson@phys.chem.ethz.ch

†xzli@pku.edu.cn

*angelos.michaelides@ucl.ac.uk

- [1] M. Nishijima, H. Okuyama, N. Takagi, T. Aruga, and W. Brenig, *Surf. Sci. Rep.* **57**, 113 (2005).
- [2] J. V. Barth, *Surf. Sci. Rep.* **40**, 75 (2000).
- [3] G. Vidali, *Chem. Rev.* **113**, 8762 (2013).
- [4] T. P. M. Goumans and J. Kästner, *Angew. Chem., Int. Ed.* **49**, 7350 (2010).
- [5] N. Lopez, Z. Lodziana, F. Illas, and M. Salmeron, *Phys. Rev. Lett.* **93**, 146103 (2004).
- [6] D. Teschner, J. Borsodi, A. Wootsch, Z. Rvay, M. Hvecker, A. Knop-Gericke, S. D. Jackson, and R. Schlögl, *Science* **320**, 86 (2008).
- [7] M. Pozzo and D. Alfè, *Int. J. Hydrogen Energy* **34**, 1922 (2009).
- [8] A. D. Jewell, G. Peng, M. F. G. Mattera, E. A. Lewis, C. J. Murphy, G. Kyriakou, M. Mavrikakis, and E. C. H. Sykes, *ACS Nano* **6**, 10115 (2012).
- [9] Z. Liang, H. J. Yang, J. Oh, J. Jung, Y. Kim, and M. Trenary, *ACS Nano* **9**, 8303 (2015).
- [10] T. S. Lin and R. Gomer, *Surf. Sci.* **255**, 41 (1991).
- [11] X. D. Zhu, A. Lee, A. Wong, and U. Linke, *Phys. Rev. Lett.* **68**, 1862 (1992).
- [12] L. J. Lauhon and W. Ho, *Phys. Rev. Lett.* **85**, 4566 (2000).
- [13] A. Jardine, H. Hedgeland, G. Alexandrowicz, W. Allison, and J. Ellis, *Prog. Surf. Sci.* **84**, 323 (2009).
- [14] G. X. Cao, E. Nabighian, and X. D. Zhu, *Phys. Rev. Lett.* **79**, 3696 (1997).
- [15] X. Wang, Y. Y. Fei, and X. D. Zhu, *Chem. Phys. Lett.* **481**, 58 (2009).
- [16] C. Z. Zheng, C. K. Yeung, M. M. T. Loy, and X. Xiao, *Phys. Rev. Lett.* **97**, 166101 (2006).
- [17] A. P. Jardine, E. Y. M. Lee, D. J. Ward, G. Alexandrowicz, H. Hedgeland, W. Allison, J. Ellis, and E. Pollak, *Phys. Rev. Lett.* **105**, 136101 (2010).
- [18] E. M. McIntosh, K. T. Wikfeldt, J. Ellis, A. Michaelides, and W. Allison, *J. Phys. Chem. Lett.* **4**, 1565 (2013).
- [19] D. Chandler and D. E. Manolopoulos, *Faraday Discuss.* **195**, 699 (2016).
- [20] H. Jónsson, *Proc. Natl. Acad. Sci. U.S.A.* **108**, 944 (2011).
- [21] T. R. Mattsson, U. Engberg, and G. Wahnström, *Phys. Rev. Lett.* **71**, 2615 (1993).
- [22] L. Y. Chen and S. C. Ying, *Phys. Rev. Lett.* **73**, 700 (1994).
- [23] W. Wang and Y. Zhao, *J. Chem. Phys.* **130**, 114708 (2009).
- [24] Y. V. Suleimanov, *J. Phys. Chem. C* **116**, 11141 (2012).
- [25] T. R. Mattsson and G. Wahnström, *Phys. Rev. B* **56**, 14944 (1997).
- [26] T. R. Mattsson and G. Wahnström, *Phys. Rev. B* **51**, 1885 (1995).
- [27] J. Kua, L. J. Lauhon, W. Ho, and W. A. Goddard III, *J. Chem. Phys.* **115**, 5620 (2001).
- [28] P. G. Sundell and G. Wahnström, *Phys. Rev. B* **70**, 081403 (2004).
- [29] T. Firmino, R. Marquardt, F. Gatti, and W. Dong, *J. Phys. Chem. Lett.* **5**, 4270 (2014).
- [30] G. Kresse and J. Furthmüller, *Phys. Rev. B* **54**, 11169 (1996).
- [31] J. P. Perdew, K. Burke, and M. Ernzerhof, *Phys. Rev. Lett.* **77**, 3865 (1996).
- [32] G. Henkelman and H. Jónsson, *J. Chem. Phys.* **113**, 9978 (2000).
- [33] Strong corner-cutting effects are not expected for the diffusion barriers studied here because of the stiff vibrational frequencies at the transition state.
- [34] P. G. Sundell and G. Wahnström, *Phys. Rev. Lett.* **92**, 155901 (2004).
- [35] R. P. Feynman and A. R. Hibbs, *Quantum Mechanics and Path Integrals* (McGraw-Hill, New York, 1965).
- [36] T. J. H. Hele and S. C. Althorpe, *J. Chem. Phys.* **138**, 084108 (2013).
- [37] I. R. Craig and D. E. Manolopoulos, *J. Chem. Phys.* **123**, 034102 (2005).
- [38] S. Habershon, D. E. Manolopoulos, T. E. Markland, and T. F. Miller, *Annu. Rev. Phys. Chem.* **64**, 387 (2013).
- [39] T. E. Markland, S. Habershon, and D. E. Manolopoulos, *J. Chem. Phys.* **128**, 194506 (2008).
- [40] T. F. Miller and D. E. Manolopoulos, *J. Chem. Phys.* **123**, 154504 (2005).
- [41] Y. Li, Y. V. Suleimanov, and H. Guo, *J. Phys. Chem. Lett.* **5**, 700 (2014).
- [42] R. Collepardo-Guevara, I. R. Craig, and D. E. Manolopoulos, *J. Chem. Phys.* **128**, 144502 (2008).
- [43] J. O. Richardson, *Faraday Discuss.* **195**, 49 (2016).
- [44] W. H. Miller, *J. Chem. Phys.* **62**, 1899 (1975).
- [45] S. Coleman, *Phys. Rev. D* **15**, 2929 (1977).
- [46] J. O. Richardson and S. C. Althorpe, *J. Chem. Phys.* **131**, 214106 (2009).
- [47] J. Kästner, *WIREs Comput. Mol. Sci.* **4**, 158 (2014).
- [48] J. O. Richardson, *J. Chem. Phys.* **144**, 114106 (2016).
- [49] S. Andersson, G. Nyman, A. Arnaldsson, U. Manthe, and H. Jónsson, *J. Phys. Chem. A* **113**, 4468 (2009).

- [50] J. B. Rommel, Y. Liu, H.-J. Werner, and J. Kästner, *J. Phys. Chem. B* **116**, 13682 (2012).
- [51] S. Álvarez-Barcia, J.R. Flores, and J. Kästner, *J. Phys. Chem. A* **118**, 78 (2014).
- [52] S. Álvarez-Barcia, M.-S. Russ, J. Meisner, and J. Kästner, *Faraday Discuss.* **195**, 69 (2016).
- [53] A. N. Beyer, J. O. Richardson, P. J. Knowles, J. Rommel, and S. C. Althorpe, *J. Phys. Chem. Lett.* **7**, 4374 (2016).
- [54] R. P. Bell, *Tunnel Effect in Chemistry* (Chapman & Hall, London, 1980).
- [55] See Supplemental Material at <http://link.aps.org/supplemental/10.1103/PhysRevLett.119.126001> for computational details, functional dependence, model details, derivations, and extended data and discussion.
- [56] N. Takagi, Y. Yasui, T. Takaoka, M. Sawada, H. Yanagita, T. Aruga, and M. Nishijima, *Phys. Rev. B* **53**, 13767 (1996).
- [57] K. Christmann, R. J. Behm, G. Ertl, M. A. V. Hove, and W. H. Weinberg, *J. Chem. Phys.* **70**, 4168 (1979).
- [58] J. Lapujoulade and K. Neil, *Surf. Sci.* **35**, 288 (1973).
- [59] G. Kresse and J. Hafner, *Surf. Sci.* **459**, 287 (2000).
- [60] G. A. Voth, D. Chandler, and W. H. Miller, *J. Chem. Phys.* **91**, 7749 (1989).
- [61] D. Chandler, *J. Chem. Phys.* **68**, 2959 (1978).
- [62] M. J. Gillan, *J. Phys. C* **20**, 3621 (1987).
- [63] M. Rossi, M. Ceriotti, and D. E. Manolopoulos, *J. Chem. Phys.* **140**, 234116 (2014).
- [64] T. J. H. Hele and Y. V. Suleimanov, *J. Chem. Phys.* **143**, 074107 (2015).
- [65] L. Kristinsdóttir and E. Skúlason, *Surf. Sci.* **606**, 1400 (2012).
- [66] V. A. Benderskii, D. E. Makarov, and C. A. Wight, *Chemical Dynamics at Low Temperatures* (Wiley, New York, 1994).